

Grand-Canonical Model of Electrochemical Double Layers from a Hybrid Density-Potential Functional

Jun Huang,^{1,,#} Shengli Chen,² Michael Eikerling^{1,3,*}*

1 Institute of Energy and Climate Research, Theory and Computation of Energy Materials (IEK-13), Forschungszentrum Jülich GmbH, 52425 Jülich, Germany

2 Hubei Key Laboratory of Electrochemical Power Sources, Key Laboratory of Analytical Chemistry for Biology and Medicine (Ministry of Education), Department of Chemistry, Wuhan University, Wuhan 430072, China.

3 Chair of Theory and Computation of Energy Materials, Faculty of Georesources and Materials Engineering, RWTH Aachen University, Aachen 52062, Germany

** Corresponding author:*

j.huang@fz-juelich.de (J.H)

m.eikerling@fz-juelich.de (M.E.)

Present address: Institute of Theoretical Chemistry, Ulm University, 89069 Ulm Germany

Abstract

A hybrid density-potential functional of an electrochemical interface that encompasses major effects in the contacting metal and electrolyte phases is formulated. Variational analysis of this functional yields a grand-canonical model of the electrochemical double layer (EDL). Specifically, metal electrons are described using the Thomas-Fermi-Dirac-Wigner theory of an inhomogeneous electron gas. The electrolyte solution is treated classically at the mean-field level, taking into account electrostatic interactions, ion size effects, and nonlinear solvent polarization. The model uses parameterizable force relations to describe the short-range forces between metal cationic cores, metal electrons as well as electrolyte ions and solvent molecules. Therefore, the gap between the metal skeleton and the electrolyte solution, key to properties of the EDL, varies consistently as a function of the electrode potential. Partial charge transfer in the presence of ion specific adsorption is described using an Anderson-Newns type theory. This model is parameterized with density functional theory calculations, compared with experimental data, and then employed to unravel several interfacial properties of fundamental significance in electrochemistry. In particular, a closer approach of the solution phase towards the metal surface, e.g. caused by a stronger ion specific adsorption, decreases the potential of zero charge and elevates the double-layer capacitance curve. In addition, the ion specific adsorption can lead to surface depolarization of ions. The present model represents a viable framework to model (reactive) EDLs under the constant potential condition, which can be used to understand multifaceted EDL effects in electrocatalysis.

1 Introduction

An electrochemical cell consists of two electrodes separated by an electrolyte solution. When the two electrodes are connected via metal wires with a potentiostat, the electric potential difference, $\Delta\phi_M$, between the two electrodes can be varied. Variation of $\Delta\phi_M$ provides a handle to control the electron flow between the two electrodes. For ideally polarizable electrodes, electron transfer reactions are prohibited regardless of $\Delta\phi_M$. Therefore, a net flow of electrons from one electrode to the other results in two electrified electrodes carrying an excess surface charge of the same magnitude but opposite sign, constituting a capacitive response. The excess electrode charge attracts via the coulombic force counterions and repels for the same reason coions in the electrolyte solution, generating a nonelectroneutral layer in the vicinity of the electrified electrode. This layer is termed the diffuse layer, whose thickness is determined by the balance between coulombic and entropic forces. The electrochemical (electric) double layer (EDL) refers to the three-dimensional interfacial region between the electrified electrode and the nearby solution. In a strict sense, the EDL is not an interface (a two-dimensional sharp boundary between two phases), but rather an interphase (a three-dimensional thin region between two phases).¹

The EDL is of central importance in electrochemistry because the potential and ion density distribution in this microscopic region determine the charging response and the charge transfer kinetics at the electrode, i.e., the phenomena that lie at the heart of electrochemistry. Albeit being the most important component in any electrochemical cell, the EDL remains notoriously difficult to grasp. The gaps in understanding are due to the fact that huge spatial variations in the electric potential, charge density and solvent polarization occur in the EDL that is only several Å to nm thick, too complex for first-principles simulation based on density functional theory (DFT), yet too thin for classical

continuum approaches. Small uncertainties in relevant physical approaches may generate huge variations in the results obtained.

Modelling the EDL has a long history which can be traced back to Helmholtz (1879) who viewed the EDL as a planar plate capacitor.² A large number of EDL models have been developed in the past, and they can be broadly divided into three categories, Gouy-Chapman-Stern (GCS) models,³⁻¹⁵ Jellium models,¹⁶⁻²⁹ and first-principle models that utilize DFT calculations.³⁰⁻³⁸ In Figure 1, we compare these three categories of EDL models in terms of the type of the statistical ensemble (canonical/grand canonical), the treatment of the electrolyte solution (implicit/explicit), and the treatment of metal electrons (implicit/explicit).

Gouy-Chapman-Stern (GCS) model is a classical EDL model which conceptualizes the EDL as a serial connection of a rigid Helmholtz plane which corresponds to the plane of the closest approach of solvated ions, and the Gouy-Chapman diffuse layer.³⁻⁵ Subsequent improvements over the GCS model take into account ion steric effects,^{6, 10-11} specific adsorption and chemisorption,^{9, 14-15, 39} solvent polarization effects that lower the dielectric permittivity of near-surface solvent layers,⁴⁰⁻⁴¹ and nonlocal short-range correlations that become increasingly nontrivial in concentrated solutions.^{12, 42-43} A commonality shared by GCS-like models is that they use a continuum description of the electrolyte region, which is essentially treated as a coulombic fluid, while the metal is treated as a featureless boundary. If the metal is treated either as a constant-potential or a constant-charge boundary, GCS-like models correspond to either a grand-canonical or a canonical ensemble. Changing the statistical ensemble from canonical to grand canonical thus implies a different boundary condition.

Jellium models are centered around metal electronic effects that are neglected in GCS-like models. The metal side is treated as an interacting inhomogeneous electron gas

situated against a positive background charge due to metal cationic cores.⁴⁴⁻⁴⁵ The principal motivation of jellium models is to understand the origin of the Helmholtz capacitance.^{16-19, 29} The electrolyte solution is simply represented by a number of dipoles interacting with metal electrons,¹⁸⁻¹⁹ or treated using the Gouy-Chapman model, e.g. ref.¹⁷. With the help of trial functions, jellium models allow approximate analytical solutions of the metal electron density and electric potential distributions under the condition of constant charge.^{22, 26}

First-principles models that utilize DFT-based calculations aim at an *ab initio* simulation of the EDL by using a set of self-consistent nonlocal integro-differential equations to solve the electronic structure problem for atoms and molecules.⁴⁶ The problem with the DFT-based approach in simulating EDLs is that it, in its default configuration, simulates a canonical system with a fixed number of particles, while the EDL is a grand-canonical ensemble with the particle densities modulated by potentials.⁴⁷⁻⁴⁸ Momentous research efforts are striving, with a varying level of success, to realize grand-canonical *ab initio* simulations of the EDL, see review articles.^{36, 38, 49} The computational costs are, at least for the moment, forbiddingly high.

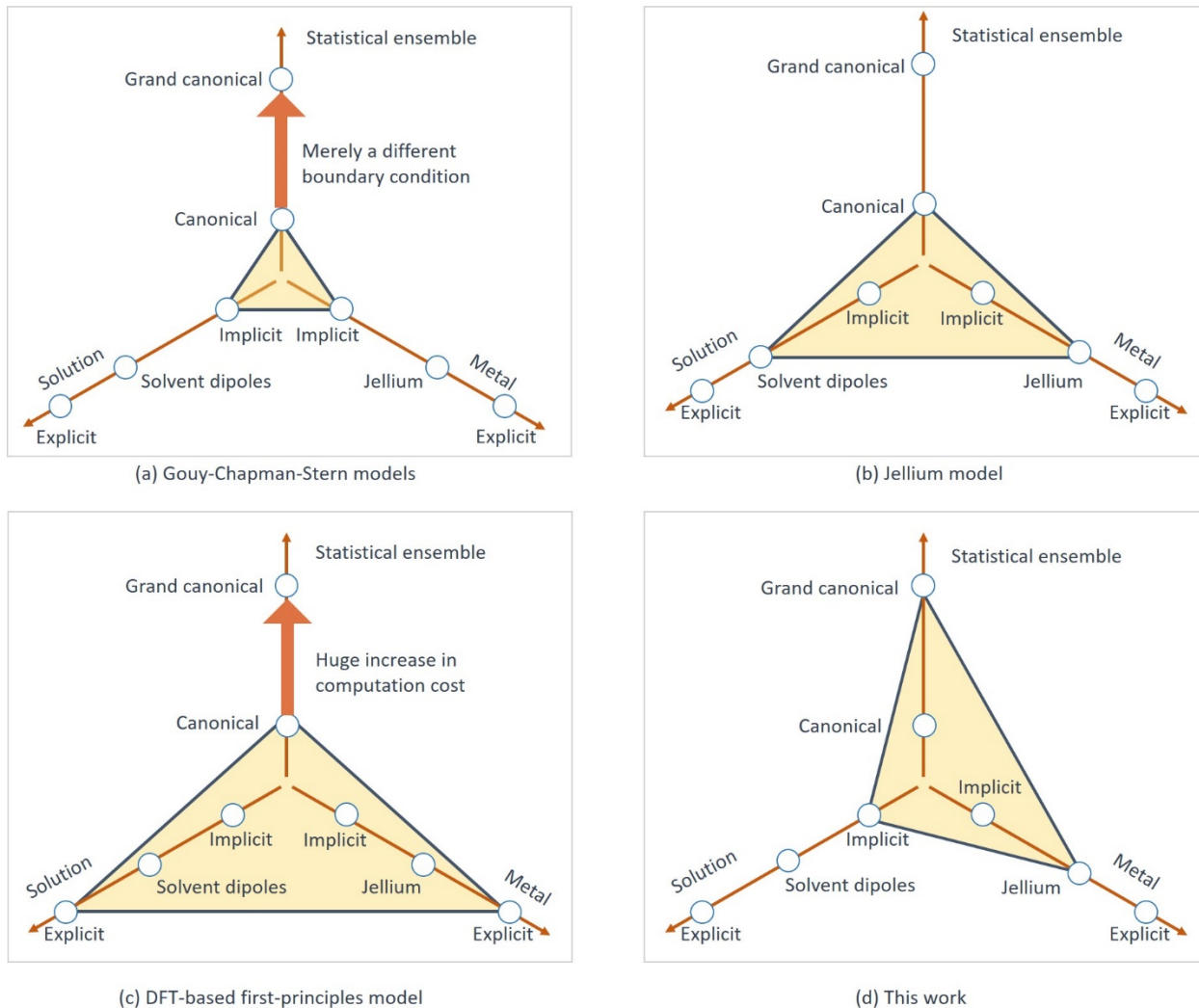


Figure 1. Comparative illustration of three categories of EDL models in three vectors corresponding to the treatment of the solution, the treatment of the metal, and the statistical ensemble: (a) Gouy-Chapman-Stern model, (b) Jellium model, (c) DFT-based first-principles model, and (d) the model developed in this work.

It is desirable to develop a grand-canonical EDL model that encompasses major effects in the contacting metal and electrolyte phases while retaining the simplicity of GCS-like models, which is the motivation of this work. An EDL model of this sort, termed Jellium-

Poisson-Boltzmann model, has been developed recently by us.⁵⁰ However, the previous model did not consider strong electronic interactions between metal electrons and solution species, thus cannot be used to describe reactive EDLs, e.g., the EDL with ion specific adsorption. In addition, the previous model used a fixed value for the width of the gap between the metal skeleton and the electrolyte solution, and neglected the discreteness of metal cationic cores. The current work improves over the previous one in these aspects. Consequently, the new model allows the metal-solution gap width to vary as a function of the metal electric potential, depicts oscillating distributions of the electric potential in the metal phase, captures key features of the EDL with ion specific adsorption, and sheds new light on several interfacial properties of fundamental significance in electrochemistry.

2 Model Development

2.1 *System specifications*

Figure 2 presents a schematic illustration of the EDL. The metal side is connected with an electron reservoir. The electrochemical potential of electrons in the metal is an independent variable, which is adjusted by varying the metal electric potential (ϕ_M). The electrolyte solution is connected with a large reservoir containing cations, anions, and solvent molecules. Cations and anions are dressed with solvation shells. Solvent molecules forming the ions' solvation shell are distinguished from unbounded ones since their orientational and translational motions are restricted. The reference value of electric potential is defined in the solution bulk, namely, $\phi_s^b = 0$ where the superscript b represents the bulk phase. The electrochemical potentials of ions and solvent molecules, denoted as $\tilde{\mu}_i$, are adjusted by varying particle concentrations, n_i^b . The volume of the EDL, V , is fixed and much smaller than that of the reservoirs. Therefore, the temperature

of the EDL is constant, T , as the EDL can exchange energy with the two large heat reservoirs. The densities of particles in the EDL are modulated by electrochemical potentials of particles in the two reservoirs via free particle exchange.

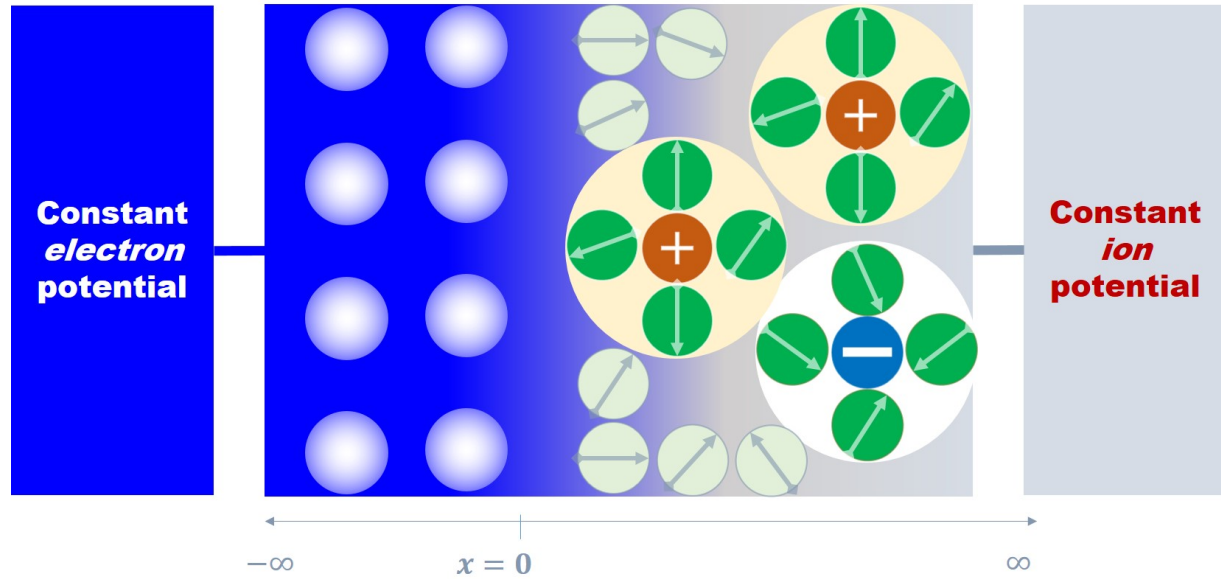


Figure 2. Schematic illustration of the EDL. The metal side is connected with an electron reservoir to hold the electrochemical potential of electrons constant. The solution side is connected with an electrolyte reservoir to hold the electrochemical potentials of ions and solvent constant. The solvation shells of cations and anions are explicitly shown. Bounded and free solvent molecules are treated separately.

Given V , T and $\tilde{\mu}_i$, with i indexing for metal electrons (e), metal cationic cores (mc), solution cations (c), solution anions (a), and solvent molecules (s), the EDL is a grand-canonical ensemble. A microstate of the EDL is defined by a certain distribution of particle densities, $\{n_i\}$. When ϕ_M varies, distributions of electric potential from the metal bulk to the solution bulk change accordingly, rearranging particle densities and the orientational configuration of solvent dipoles. The primary target of the present model

is to obtain the distributions of electric potential and particle densities in the EDL as a function of ϕ_M , from which the surface free charge density and the double-layer capacitance can be derived.

The probability of finding a grand-canonical ensemble in a microstate with particle densities $\{n_i\}$ is given by,

$$p(\{V, T, \{\tilde{\mu}_i\}, \{n_i\}\}) = \frac{1}{Z} \exp(-\beta\Omega), \quad (1)$$

where $\beta = (k_B T)^{-1}$, Z is a normalization factor, and Ω is the grand potential, expressed as,

$$\Omega(\{V, T, \{\tilde{\mu}_i\}, \{n_i\}\}) = U - TS - \int dV \tilde{\mu}_i n_i, \quad (2)$$

with U being the internal, S the entropy, dV a volume unit of the space.

The most probable microstate of the EDL corresponds to the minimum of Ω . The relative fluctuation of particle numbers deviating from the most probable microstate varies as $(N)^{-\frac{1}{2}}$ with N being the number of particles in the EDL.⁵¹ In actual situations, N is on the order of N_A (Avogadro constant), thus the relative fluctuation is, for practical consideration, infinitesimal and can be neglected.

2.2 Grand potential with approximations

The task of describing the EDL is translated thus to that of obtaining the minimum of $\Omega(\{V, T, \{\tilde{\mu}_i\}, \{n_i\}\})$. To this end, an explicit expression of $\Omega(\{V, T, \{\tilde{\mu}_i\}, \{n_i\}\})$ is needed. As the EDL is a large-size, quantum many-body system, approximations are required, on varying levels, for any workable calculation. In the following, we treat first U and then S .

The total internal energy of the EDL is the sum of kinetic energy and potential energy of all particles interacting with each other. In line with the Born–Oppenheimer approximation, the nuclear kinetic energy is neglected in the electronic Hamiltonian. The solution side is treated as a collection of charged particles and solvent dipoles in the context of classical electrostatics. Short-range interactions between the metal and solution species are described using parameterizable force fields.

The total internal energy can be decomposed into four terms,

$$U = T_{\text{ni}}[n_e, \nabla n_e, \dots] + U_{\text{xc}}[n_e, \nabla n_e, \dots] + U_{\text{es}}[\{n_i\}, \phi, \nabla \phi] + U_{\text{nu}}[\vec{r}, \{n_i\}] + U_{\text{ion}}[\{n_i\}], \quad (3)$$

$T_{\text{ni}}[n_e, \nabla n_e, \dots]$ is the kinetic energy of metal electrons, which is a functional of the metal electron density, n_e , and its gradients, ∇n_e , $\nabla^2 n_e$, etc. Herein, we adopt the extended Thomas-Fermi theory with the lowest-order gradient correction,⁵²⁻⁵⁴

$$T_{\text{ni}}[n_e, \nabla n_e, \dots] = \int dV \xi a_0^2 \left(c_1 n_e^{\frac{5}{3}} + c_2 \frac{(\nabla n_e)^2}{n_e} \right), \quad (4)$$

where a_0 is the Bohr radius, $\xi = e_0^2/(4\pi\epsilon_0 a_0)$ is the reference energy with e_0 being the unit of electrical charge, and ϵ_0 is the vacuum permittivity; $c_1 = \frac{3}{10} (3\pi^2)^{\frac{2}{3}}$ and $c_2 = \frac{1}{72}$ are two coefficients.

$U_{\text{xc}}[n_e, \nabla n_e, \dots]$ is the exchange-correlation energy, which is approximated as,⁵²

$$U_{\text{xc}}[n_e, \nabla n_e, \dots] = \int dV \xi a_0 \left(c_3 n_e^{\frac{4}{3}} + c_4 n_e^{\frac{4}{3}} \frac{1}{c_5 + a_0 n_e^{\frac{1}{3}}} \right), \quad (5)$$

where the first term in the bracket, with $c_3 = -\frac{3}{4}\left(\frac{3}{\pi}\right)^{\frac{1}{3}}$, represents the exchange energy of a uniform electron gas, the second term, with $c_4 = -0.056$, $c_5 = 0.079$, is Wigner's classical result.⁵⁵

Eqs. (4) and (5) constitute the Thomas-Fermi-Dirac-Wigner (TFDW) theory of the inhomogeneous electron gas, which is the progenitor of modern density functional theory (DFT).^{56, 57} As for the Ag(111)-vacuum system, we compare the present model based on TFDW theory with modern DFT calculations in *Figure S1 in the Supporting Information*. Our results show that the TFDW theory does a sufficient job of describing the distributions of electron density and electric potential in the metal bulk and near the metal surface, which is in line with jellium models for metal surfaces.^{26, 29, 44-45, 56} The main deficiency of the TFDW lies in the treatment of the exchange-correlation energy, U_{xc} , which, albeit being a relative small fraction of the total energy, is very important for chemical bond formation.⁴⁶ In this work, this problem is amended expediently by using the Anderson-Newns theory of chemisorption.⁵⁷⁻⁵⁸

$U_{es}[\{n_i\}, \phi, \nabla\phi]$ is the electrostatic potential energy of the EDL,^{11, 50}

$$U_{es}[\{n_i\}, \phi, \nabla\phi] = \int dV \left(-\frac{1}{2}\epsilon_{\infty}E^2 + e_0\phi \left[\sum_{i=e,mc,a,c} z_i n_i \right] - n_s k_B T \ln \left[\frac{\sinh(\beta p E)}{\beta p E} \right] \right), \quad (6)$$

where $E = |\nabla\phi|$ is the absolute value of the electric field, ϵ_{∞} the optical permittivity, z_i the charge number, and p the dipole moment of solvent molecules. In general, the z_i parameters are position-dependent due to short-range electronic interactions with the metal. This electrosorption phenomenon will be considered in the Section 3.3.

The first term in bracket in Eq.(6) represents the self-energy of the electric field, the second term the electrostatic potential energy of charged particles, the third term the energy of solvent molecules interacting with the electric field. The third term is obtained, with the deduction detailed in *Supporting information*, from a canonical ensemble of solvent dipoles at the mean-field level. Eq.(6) is identical to the result derived from statistical field considerations at the mean field level, see Budkov.⁵⁹⁻⁶⁰

$U_{\text{nu}}[\vec{r}, \{n_i\}]$ describes repulsive forces between nuclei in metal and solution phases, which is responsible for the structure integrity of the EDL by preventing the solution species from entering the metal skeleton,

$$U_{\text{nu}}[\vec{r}, \{n_i\}] = \int dV (n_a W_a(\vec{r}) + n_c W_c(\vec{r}) + n_s W_s(\vec{r})), \quad (7)$$

and $W_i(\vec{r})$ are parameterizable, short-range, repulsive forces, which are given by a power law in the spirit of the Lennard-Jones potential,

$$W_i(\vec{r}) = \omega_i \left(\frac{\sigma_i^1}{(x - l_M) \cdot h(x - l_M) + \sigma_i^2} \right)^6, \quad (8)$$

where ω_i is positive and characterizes the force strength, σ_i^1 and σ_i^2 are two lengths characterizing the range of the interaction, x is the through-plane coordinate, l_M is the thickness of the metal phase, and $h(x)$ is the Heaviside function.

$U_{\text{ion}}(\{n_i\})$ describes ion-specific interactions between metal electrons and the electrons of solution ions. It is assumed to be a bilinear functional of the metal electron density n_e and the ion densities n_a and n_c ,

$$U_{\text{ion}}[\{n_i\}] = \int dV (n_a V_a + n_c V_c) n_e, \quad (9)$$

where V_a and V_c characterize the repulsions between metal electrons and anions/cations, respectively.

At this point, the four interaction energy terms in Eq.(3) have been obtained. Next, we will develop expressions for the entropy S . The total entropy S is composed of three contributions,

$$S = S_e + S_c + S_o, \quad (10)$$

where S_e is the entropy of metal electrons, S_o the orientational entropy of solvent molecules, and S_c the configurational entropy of ions and solvent molecules in solution. The distribution of metal electrons is only slightly altered by potential, see Figure 5. Consequently, S_e is nearly constant as ϕ_M changes. Furthermore, S_o has been considered in the energy of solvent molecules in Eq. (6). Therefore, our focus is on S_c , which is calculated from the lattice-gas model,

$$S_c = \sum k_B \ln P. \quad (11)$$

Here, we divide the solution phase into volume units of δV . The total entropy is the sum of that of all the volume units. The volume unit has $n_0 \delta V$ lattice cells, with n_0 being the lattice cell density, which are occupied by $n_c \delta V$ cations, $n_a \delta V$ anions, $n_s \delta V$ solvent molecules, and $n_v \delta V$ vacant cells. P is the number of ways all particles in the volume unit could be arranged, calculated as

$$P = \frac{(n_0 \delta V)!}{(n_c \delta V)! (n_a \delta V)! (n_s \delta V)! (n_v \delta V)!}. \quad (12)$$

Using the Stirling formula and taking the continuous limit (transforming the summation to a volume integration) yield,

$$S_c = - \int dV k_B \left(n_c \ln \frac{n_c}{n_0} + n_a \ln \frac{n_a}{n_0} + n_s \ln \frac{n_s}{n_0} + n_v \ln \frac{n_v}{n_0} \right), \quad (13)$$

where $n_v = n_0 - n_c - n_a - n_s$ is the number density of vacancies.

2.3 Controlling equations of electric potential and electron density

Combined, the grand potential is written as a volume integration of a grand potential density over the EDL,

$$\Omega = \int dV f[n_i, \nabla n_i, \phi, E], \quad (14)$$

with the volumetric density of the grand potential given by,

$$\begin{aligned} f = & t_{ni}[n_e, \nabla n_e] + u_{xc}[n_e, \nabla n_e] + e_0 \phi \sum_{i=e,mc,a,c} z_i n_i - \frac{1}{2} \epsilon_\infty E^2 \\ & - \frac{n_s}{\beta} \ln \left[\frac{\sinh(\beta p E)}{\beta p E} \right] + \frac{1}{\beta} \sum_{j=a,c,s,v} n_j \ln \frac{n_j}{n_0} \\ & + \sum_{m=a,c,s} n_m W_m + (n_a V_a + n_c V_c) n_e - \sum_{q=e,a,c,s,v} \tilde{\mu}_q n_q, \end{aligned} \quad (15)$$

where t_{ni} and u_{xc} are the volumetric densities of T_{ni} and U_{xc} , respectively. It can be seen that f is a functional of number densities, $\{n_i\}$, and electric potential, ϕ , and it is termed therefore a hybrid density-potential functional. By means of the variational procedure, we obtain Euler-Lagrange equations in terms of $\{n_i\}$ and ϕ ,

$$\frac{\partial f}{\partial X} - \nabla \cdot \left(\frac{\partial f}{\partial (\nabla X)} \right) = 0, \quad (16)$$

where $X = \phi, n_e, n_a, n_c, n_s$.

Substituting Eq.(15) into Eq.(16) with $X = \phi$ yields,

$$-\nabla \cdot [\epsilon_{\text{eff}}(n_s, E)E] = e_0 \sum_{i=e,mc,a,c} z_i n_i, \quad (17)$$

where $\epsilon_{\text{eff}}(n_s, E)$ is an effective dielectric permittivity,

$$\epsilon_{\text{eff}}(n_s, E) = \epsilon_\infty + \frac{n_s p}{E} \left[\coth(\beta p E) - \frac{1}{\beta p E} \right], \quad (18)$$

which asymptotically approaches ϵ_∞ in a strong electric field ($|\beta p E| \gg 1$) and $\epsilon_\infty + \frac{n_s \beta p^2}{3}$ in a weak electric field ($|\beta p E| \ll 1$).

Substituting Eq.(15) into Eq.(16) with $X = n_e$ yields

$$\nabla \left[\frac{\partial(t_{ni} + u_{xc})}{\partial \nabla n_e} \right] = \frac{\partial(t_{ni} + u_{xc})}{\partial n_e} + (n_a V_a + n_c V_c) - e_0 \phi - \tilde{\mu}_e, \quad (19)$$

where $\tilde{\mu}_e$ is the electrochemical potential of metal electrons.

For the expressions of t_{ni} and u_{xc} used in this theory, we have

$$\frac{\partial(t_{ni} + u_{xc})}{\partial \nabla n_e} = 2\xi a_0^2 c_2 \frac{\nabla n_e}{n_e}, \quad (20)$$

$$\frac{\partial(t_{ni} + u_{xc})}{\partial n_e} = \xi a_0^2 \left(\frac{5}{3} c_1 n_e^{\frac{2}{3}} - c_2 \frac{(\nabla n_e)^2}{(n_e)^2} \right) + \xi a_0 \left(\frac{4}{3} c_3 n_e^{\frac{1}{3}} + c_4 \frac{n_e^{\frac{1}{3}} \left(\frac{4}{3} c_5 + a_0 n_e^{\frac{1}{3}} \right)}{\left(c_5 + a_0 n_e^{\frac{1}{3}} \right)^2} \right). \quad (21)$$

Substituting Eq.(15) into Eq.(16) with $X = n_a, n_c, n_s$ gives

$$\begin{aligned}
z_a e_0 \phi + \frac{1}{\beta} \ln \frac{n_a}{n_0 - n_a - n_c - n_s} + W_a + V_a n_e - \tilde{\mu}_a &= 0, \\
z_c e_0 \phi + \frac{1}{\beta} \ln \frac{n_c}{n_0 - n_a - n_c - n_s} + W_c + V_c n_e - \tilde{\mu}_c &= 0, \\
-\frac{1}{\beta} \ln \left[\frac{\sinh(\beta p E)}{\beta p E} \right] + \frac{1}{\beta} \ln \frac{n_s}{n_0 - n_a - n_c - n_s} + W_s - \tilde{\mu}_s &= 0,
\end{aligned} \tag{22}$$

which leads to

$$n_{c,a,s} = n_0 \frac{\chi_{c,a,s} \theta_{c,a,s}}{\chi_v + \theta_a \chi_a + \theta_c \chi_c + \theta_s \chi_s}, \tag{23}$$

with $\chi_{c,a,s,v}$ being the fractions of cations, anions, solvent molecules, and vacancies in the solution bulk, and $\theta_{c,a,s}$ being spatially dependent Boltzmann factors

$$\begin{aligned}
\theta_{c,a} &= \exp(-z_{c,a} e_0 \beta \phi - \beta W_{c,a} - \beta V_{c,a} n_e), \\
\theta_s &= \exp\left(\ln \left[\frac{\sinh(\beta p E)}{\beta p E} \right] - \beta W_s\right).
\end{aligned} \tag{24}$$

The fact that particles have varying sizes can be considered by modifying Eq.(23) to

$$n_{c,a,s} = n_0 \frac{\chi_{c,a,s} \theta_{c,a,s}}{\chi_v + \gamma_a \theta_a \chi_a + \gamma_c \theta_c \chi_c + \theta_s \chi_s}, \tag{25}$$

where the sizes of solvent molecules and vacancies are assumed to be equal and taken as the reference size, γ_a and γ_c denote the relative sizes of solvated anions and cations, respectively, which are calculated as

$$\gamma_{a,c} = \left(\frac{d_{a,c}}{d_s} \right)^3, \tag{26}$$

with $d_{a,c}$ being the effective diameters of anions and cations, and d_s the diameter of solvent molecules. We have $d_c = 2r_c + 2d_s$ for cations assuming a spherical solvation shell consisting of a single layer of solvent molecules, where r_a is the radius of bare cations. Since the anion-solvent interactions are much weaker than cation-solvent interactions,⁶¹⁻⁶³ we do not designate a fixed solvation shell for anions; instead, we use $d_c = 2r_a$ with r_a representing the radius of bare anions. A more rigorous treatment of the size effect has been presented by Zhang and Huang,⁶⁴ resulting in transcendental equations that cannot be solved analytically. The present consideration in Eq.(25) is simple, intuitive, and gives correct asymptotic behavior. When $\theta_{a,c} \rightarrow \infty$, namely, when anions or cations dominate in the solution phase, Eq.(25) is asymptotic to $n_{a,c} = \frac{n_0}{\gamma_{a,c}}$.

Substituting density expressions given in Eq.(25) into Eq.(17) results in a second-order ordinary differential equation (ODE) in ϕ . Combined, Eqs.(17) and (19) constitute a closed set of controlling equations to solve for the density and electric potential distributions in the EDL. The presented formalism eliminates the need of trial functions for the electron density profile, which was the standard procedure in the vast majority of previous studies employing a jellium model to describe metal electronic effects in the EDL.^{17-18, 26, 29} Uncertainties introduced in trial functions are thus eliminated.

2.4 Boundary conditions

Eqs.(17) and (19) are closed with boundary conditions (BCs) as follows. The BCs on the solution side at far distance from the EDL are,

$$\phi = 0, \quad n_e = 0, \quad (27)$$

where the first identity corresponds to the use of the electric potential in the solution bulk as the potential reference, and the second identity reflects the fact that metal electrons are absent in the solution bulk.

The BCs on the metal side far away from the EDL are dependent on how the metal cationic cores are considered. In the simplest case, metal cationic cores are treated as a uniform background of positive charge density n_{mc} , then the BCs on the metal side follow,

$$\phi = \phi_M, \quad n_e = n_{mc}. \quad (28)$$

In Eq.(28), the metal electric potential is explicitly given in the BC. Consequently, constant-potential modulation of the EDL is apparently achieved.

For the case where the size and arrangement of metal cationic cores are explicitly considered, we can take the metal-side boundary at the central plane of metal cationic cores. Consequently, symmetrical BCs apply,

$$\nabla\phi = 0, \quad \nabla n_e = 0. \quad (29)$$

For this case, the metal electric potential plays its role by affecting $\tilde{\mu}_e$ in Eq. (19), which is calculated as,

$$\tilde{\mu}_e = \mu_e - e\phi_M, \quad (30)$$

where μ_e is the chemical potential of metal electrons, which is calculated from Eq.(19).

2.5 Nondimensionalization, numerical implementation, and parameters

We define dimensionless variables, marked with an over-bar, as follows,

$$\bar{n}_i = n_i(a_0)^3, \bar{x} = \frac{x}{a_0}, \bar{\phi} = \frac{e_0}{k_B T} \phi, \bar{p} = \frac{p}{e_0 a}, \quad (31)$$

which refer to the normalized number density, length, electric potential, and dipole moment, respectively. The modified Poisson-Boltzmann equation in Eq.(17) is rewritten in dimensionless variables as,

$$-\nabla(\bar{\epsilon}_\infty \nabla \bar{\phi} + \bar{n}_s \bar{p} \kappa \mathcal{L}) = \kappa \left(\sum_{i=e,mc,a,c} z_i \bar{n}_i \right), \quad (32)$$

where $\kappa = \frac{e_0^2}{k_B T \epsilon_0 a_0}$ is a number derived from fundamental constants, and $\mathcal{L} = \coth(\bar{p} \bar{E}) - \frac{1}{\bar{p} \bar{E}}$.

The dimensionless form of Eq.(19) for the metal electron density reads,

$$\begin{aligned} \nabla^2 \bar{n}_e = & \frac{1}{2\bar{n}_e} (\nabla \bar{n}_e)^2 + \frac{\bar{n}_e}{2c_2} (\bar{\mu}_e(\bar{n}_e) - \bar{\mu}_e(\bar{n}_e^0)) \\ & - \frac{2\pi}{\kappa c_2} \bar{n}_e (\bar{\phi} - \bar{\phi}_M - \bar{V}_a \bar{n}_a - \bar{V}_c \bar{n}_c), \end{aligned} \quad (33)$$

where $\bar{\mu}_e$ is the dimensionless chemical potential of metal electrons. For a homogeneous electron gas described by the TFDW theory, $\bar{\mu}_e(\bar{n}_e)$ is calculated as,

$$\bar{\mu}_e(\bar{n}_e) = \frac{5}{3} c_1 (\bar{n}_e)^{\frac{2}{3}} + (\bar{n}_e)^{\frac{1}{3}} \left(\frac{4}{3} c_3 + c_4 \frac{\frac{4}{3} c_5 + (\bar{n}_e)^{\frac{1}{3}}}{\left(c_5 + (\bar{n}_e)^{\frac{1}{3}} \right)^2} \right) \quad (34)$$

Eqs. (32) and (33) constitute the dimensionless controlling equations of the present theory. Technical details on numerical implementation using the 'bvp4c' solver in Matlab⁶⁵ are provided in *Supporting Information*.

In a previous work, we have studied the case where the metal is treated as a jellium with a uniform charge background.⁵⁰ In this work, we consider a one-dimensional, discrete, periodic arrangement of metal cationic cores, as depicted in Figure 3, which represents a step closer to the real situation. The charge distribution of metal cationic cores is written as,

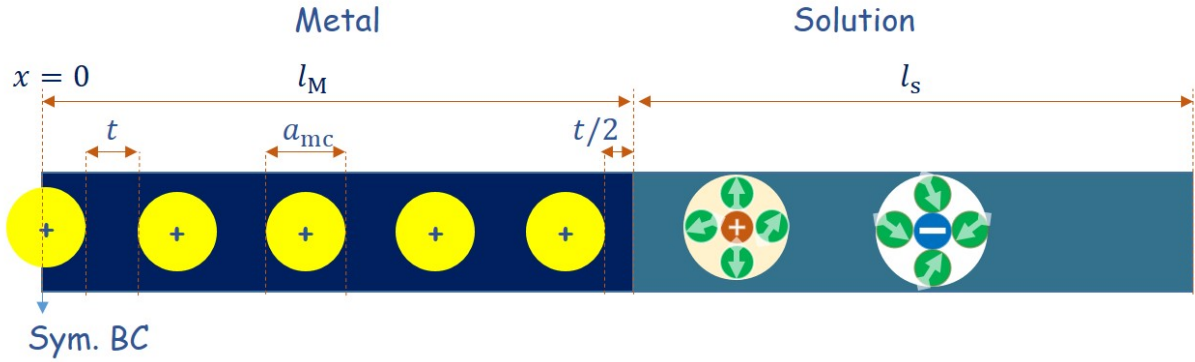
$$\frac{\bar{n}_{mc}(x)}{\bar{n}_{mc}^0} = h(x) - h\left(x - \frac{a_{mc}}{2}\right) + h\left(x - \frac{a_{mc}}{2} - t\right) - h\left(x - \frac{3a_{mc}}{2} - t\right) \quad (35)$$

$$+ h\left(x - \frac{3a_{mc}}{2} - 2t\right) - h\left(x - \frac{5a_{mc}}{2} - 2t\right) + h\left(x - \frac{5a_{mc}}{2} - 3t\right)$$

$$- h\left(x - \frac{7a_{mc}}{2} - 3t\right) + h\left(x - \frac{7a_{mc}}{2} - 4t\right) - h\left(x - \frac{9a_{mc}}{2} - 4t\right)$$

where $h(x) = 1$ if $x > 0$ and $h(x) = 0$ elsewhere. a_{mc} is the diameter of metal cationic cores, t the gap between two metal cationic cores, \bar{n}_{mc}^0 the normalized charge density of metal cationic cores. A symmetric boundary is applied at $x = 0$, where the BCs expressed in Eq.(29) are applied.

(a) 2D schematic illustration



(b) 1D profile

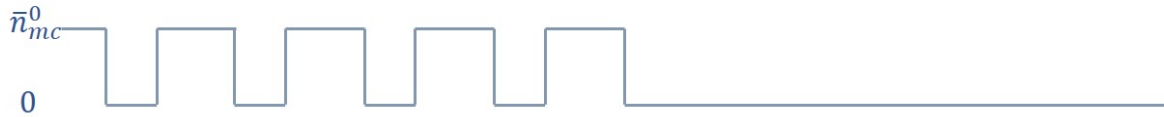


Figure 3. Schematic illustration of the distributions of (a) metal cationic cores and (b) metal cationic charge profile. a_{mc} is the diameter of metal cationic cores, t the gap between two metal cationic cores, \bar{n}_{mc}^0 the normalized charge density of metal cationic cores. The thickness of the metal phase is $l_M = 4.5(a_{mc} + t)$. Though a 2D schematic

illustration is shown in (a), the model is solved in a one-dimensional geometry where the one-dimensional metal cationic charge profile is shown in (b).

Model parameters for the base case without electrosorption, corresponding to Ag(111) in 0.1 M KPF₆, are summarized in Table 1, which are categorized into types of ‘general constants’, ‘solution’, ‘metal’, and ‘metal-solution interaction’. The solution parameters correspond to 0.1 M KPF₆ aqueous solution. The lattice size is taken as that of water molecules. Normalized number densities of cations and anions in the bulk solution are given by, $\bar{n}_a = \bar{n}_c = c_b N_A (a_0)^3$, and their bulk fractions are calculated as, $\chi_a = \chi_c = c_b N_A (d_s)^3$. In a continuum description of the EDL, all particles shall have number densities everywhere. Consequently, a fraction of unoccupied lattice cells, $\gamma_v = 0.05$, is introduced in the solution bulk, and γ_v grows to nearly unity in the metal-solution gap. As for water molecules, its bulk number density is 55.6M, its bulk dielectric constant is 78.5, and its effective dipole moment, p , is determined as 4.84D.

As for the metal, its properties are defined by four parameters, two structural parameters, a_{mc} and t , the normalized charge density of metal cationic cores \bar{n}_{mc}^0 , and the optical dielectric constant $\bar{\epsilon}_\infty^M$. Their values in Table 1 correspond to Ag(111), which are parameterized using DFT calculations in the *Supporting Information*. The optical dielectric constant shall be continuous from the metal bulk to the solution bulk, because a discontinuity of the dielectric constant will result in an induced surface charge density on the metal surface, so-called image charge effects.

Parameters in Eq.(8) describing the metal-solution interactions determine the thickness of the metal-solution gap, t_{msg} , which is obtained readily from ab initio molecular dynamics (AIMD) simulations, see ref.^{35, 37}. t_{msg} is the primary parameter determining the Helmholtz capacitance, which can be obtained using electrochemical impedance

measurements. The values listed in Table 1 result in $t_{\text{msg}} \approx 2 \text{ \AA}$, which is close to AIMD results.^{35, 37} In the base case, we assume \bar{V}_i ($i = c, a$) = 0.

Table 1 Model parameters for the base case

| Category | Symbol | Item | Value |
|-------------------|-----------------------------|--|---|
| General constants | R | Ideal gas constant | $8.314 \text{ J K}^{-1} \text{ mol}^{-1}$ |
| | k_B | Boltzmann constant | $1.38 \cdot 10^{-23} \text{ J/K}$ |
| | T | Temperature | 298.15 K |
| | e | Elementary charge | $1.6 \times 10^{-19} \text{ C}$ |
| | N_A | Avogadro's number | $6.02 \times 10^{23} / \text{mol}$ |
| | ϵ_0 | Vacuum permittivity | $8.85 \times 10^{-12} \text{ F/m}$ |
| | a_0 | Bohr radius | $5.29 \times 10^{-11} \text{ m}$ |
| | n_{ref} | Reference number density | $(a_0)^{-3}$ |
| | κ | Dimensionless constant | $e_0^2 / (k_B T \epsilon_0 a_0)$ |
| Solution | c_b | Bulk ion concentration | 0.1 M |
| | $\bar{\epsilon}_{\infty}^S$ | Optical dielectric constant of solution | 2 |
| | r_c | Cation radius | 1.38 \AA |
| | r_a | Anion radius | 3 \AA |
| | γ_c | Relative size of solvated cations | $(2r_c + 2d_s)^3 / (d_s)^3$ |
| | γ_a | Relative size of solvated anions | $(2r_a)^3 / (d_s)^3$ |
| | z_a | Charge number of anions | -1 |
| | z_c | Charge number of cations | 1 |
| | \bar{n}_s | Solvent number density | $5.56 \times 10^4 N_A (a_0)^3$ |
| | χ_v | Volume fraction of vacuum in solution bulk | 0.05 |
| | d_s | Water diameter | 2.75 \AA |
| | p_s | Water dipole moment | 4.74 D |
| Metal | \bar{n}_{mc}^0 | Dimensionless metal electron density | 0.2042 |
| | a_{mc} | Diameter of metal cationic cores | 1.10 \AA |

| | | | |
|----------------------------|-----------------------------|---|------------|
| | t | Gap between two metal cationic cores | 1.25 Å |
| | $\bar{\epsilon}_{\infty}^M$ | Optical dielectric constant of metal | 2 |
| Metal-solution interaction | ω_i (i=s,c,a) | Force constant of metal-solvent/cation/anion repulsion | $10 k_B T$ |
| | \bar{V}_i (i=c,a) | Dimensionless force constant between metal electrons and anions/cations | 0 |
| | σ_i^1 (i=s,c,a) | Characteristic length of metal-solvent/cation/anion repulsion | 2 Å |
| | σ_i^2 (i=s,c,a) | Characteristic length of metal-solvent/cation/anion repulsion | 0.4 Å |

3 Results and Discussion

3.1 Distributions of electric potential, dielectric constant, and number densities

The model is employed to describe the EDL for the base case without electrosorption, using parameters given in Table 1 corresponding to a Ag(111) in 0.1 M KPF₆. The model is solved for a one-dimensional geometry for a series of metal electric potential (U_M ranges from 1230 to 1170 with a step of 1)^①, and the resulting distributions of the electric potential, the number densities of particles (electron, anion, cation, solvent), and the dielectric constant are shown in Figure 5 and Figure 6. Due to the discreteness of metal cationic cores, the electric potential and electron density oscillate in the metal phase. The electron density extends beyond the metal skeleton ($x = l_M$), and spreads into the solution compartment, which is termed 'electron spillover'. The electron

① This potential range is used because the metal surface charge transitions from positive to negative values as the metal electric potential decreases in this range, namely, the potential of zero charge lies in this potential range. For different metals with different values of \tilde{n}_{mc}^0 , different potential ranges should be used.

spillover extends over $\sim 2 \text{ \AA}$, and is modulated slightly by ϕ_M . Specifically, decreasing ϕ_M , namely, elevating the electrochemical potential of metal electrons, pushes metal electrons further into the solution compartment.

Though the change in the electron density is slight, the electric potential distribution in the solution compartment shows a strong dependence on ϕ_M , as observed in Figure 4 (c) and (d), with variations on the order of 1.0 V. In general, the electric potential changes drastically in the near-metal region, i.e. for $1 < x < 1.2 \text{ nm}$, followed by a gradual change in the diffuse layer that extends over several nanometers and then approaching zero in the solution bulk. The sign of the electric potential changes as a function of ϕ_M , which implies that the excess free charge on the metal surface changes its sign as a function of ϕ_M .

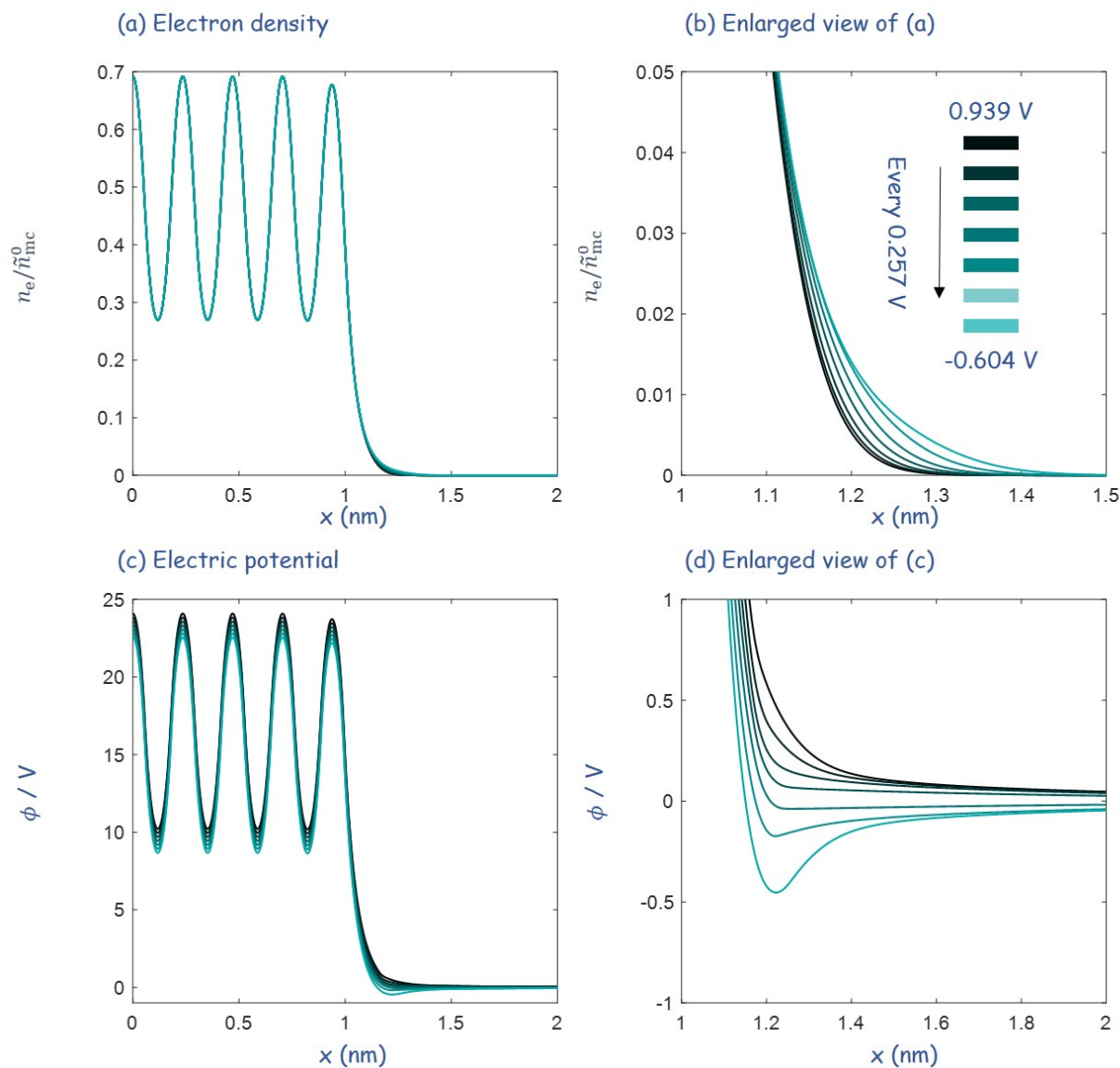


Figure 4. (a) Electron density and (c) electric potential distributions across the metal-solution interface at a series of metal electric potentials. With the potential of zero charge (pzc) as the reference, the metal electric potential varies from -0.604 V ($U_M=1170$) to 0.939 V ($U_M=1230$) (every $10k_B T/e_0 = 0.257$ V). (b) is an enlarged view of (a) in the solution region. (d) is an enlarged view of (c) in the solution region.

Cations (anions) are attracted by columbic interactions to the diffuse layer when the electric potential is locally negative (positive). Consequently, anions are accumulated in

the diffuse layer when ϕ_M is high, while depleted when ϕ_M gets lower, as shown in Figure 5 (a). The opposite trend applies for cations. The ion size effect results in a plateau in the cation density profile, signifying saturation of the cation density, in the diffuse layer, e.g. see the curve of $\phi_M = -0.604$ V vs. the potential of zero charge (pzc). The ion saturation phenomenon in the diffuse layer can be readily appreciated from Eq.(25). The maximum cation density is, $n_{c,a}^{\max} = n_0/\gamma_{c,a}$, which is obtained when $\theta_{c,a}$ dominates in the denominator of Eq.(25).

Due to volume exclusion of counterions, the number density of solvent molecules generally decreases in the diffuse layer, see Figure 5 (c). Of note, small humps in the number density of solvent molecules are found near the metal surface because solvent molecules can more effectively screen the electric field than counterions. The decreased number density of solvent molecules and the polarization saturation induced by the high local electric field together result in a sharp decrease of the dielectric constant in the diffuse layer. In several DFT studies using an implicit treatment of the solvent, the permittivity decrease in the interfacial region is described using the Fattbert-Gygi relation, which is an empirical relation expressing the permittivity as a function of the metal electron density.⁶⁶⁻⁶⁸ Aside from the uncertainties in the empirical coefficients,⁶⁹ the primary deficiency of the Fattbert-Gygi relation is the lack of physical significance. Consequently, it cannot capture the humps as seen in Figure 5 (c).

All particle number densities in Figure 5 drop to zero at ~ 2 Å away from the metal surface due to the short-range repulsive forces in Eq.(8). Consequently, a nearly-vacuum gap between the metal surface and the solution phase is formed. The gap width develops, in a consistent manner, as a function of ϕ_M (or the metal surface charge density σ_M). As the particle number densities vary continuously, we cannot define an exact location of the plane corresponding to the closest approach of particles. In general, the 'closest' approach of anions shifts further away from the metal surface, as

ϕ_M decreases, while the opposite applies for cations, see the insets of Figure 5 (a) and (b). It has been shown that the width of the metal-solution gap is crucial to the surface charging relation and the double-layer capacitance of the EDL.^{20, 24, 50, 70} Some previous works assumed a constant value for the vacuum-gap width,¹⁶⁻¹⁸ while other works tried to determine the vacuum-gap width by minimizing the grand potential^{20, 50, 70} or by using a force balance equation.²⁴ Compared to these previous treatments, our approach is simpler because it removes the need of calculating the model at a series of the gap width or an additional controlling equation of the force balance. Moreover, it is more general because, with appropriate parameterization of the force relations using DFT calculations, Eq.(8) may well describe a wide array of EDLs.

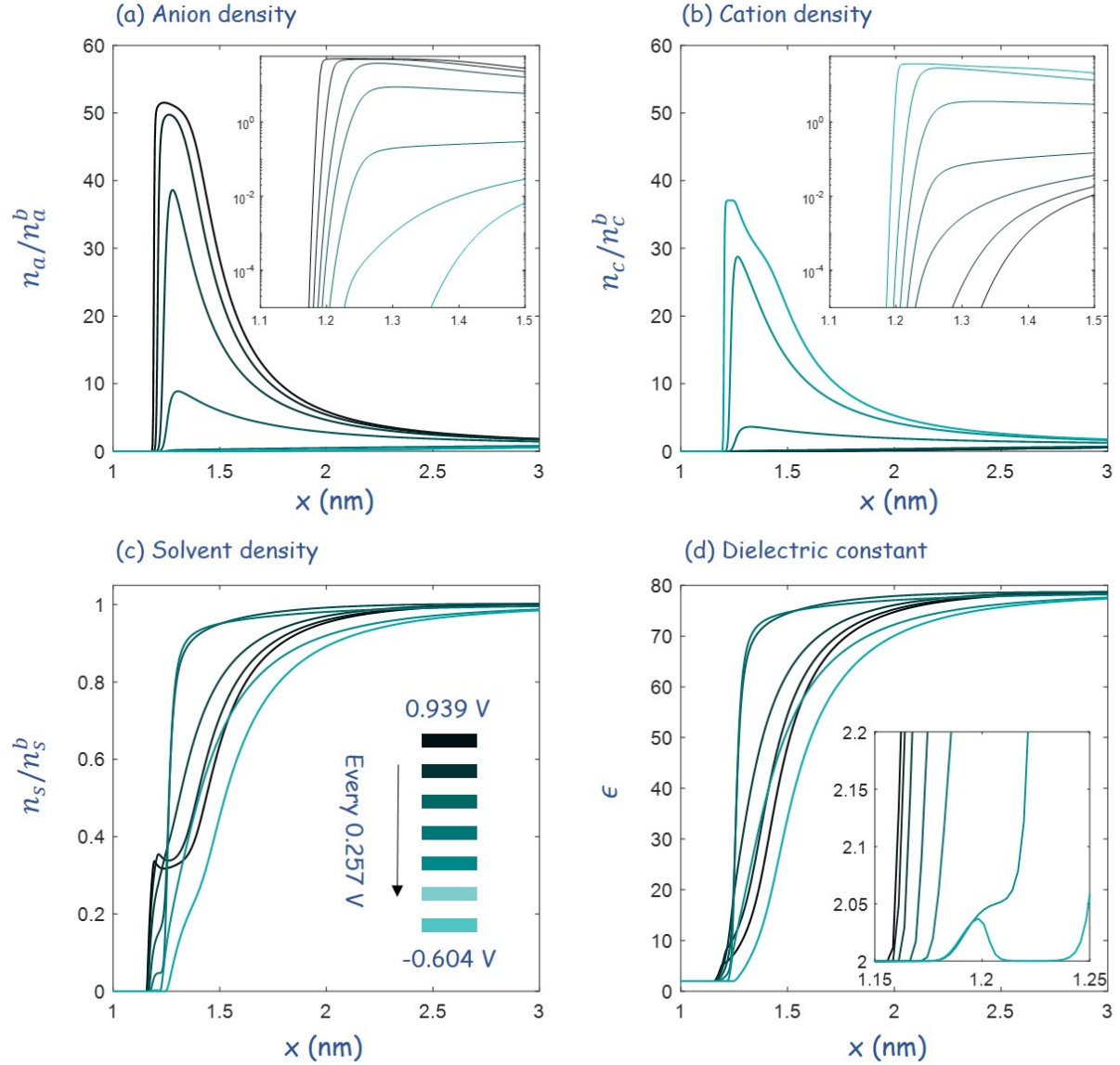


Figure 5. (a) Anion density, (b) cation density, (c) solvent density, and (d) dielectric constant across the EDL as a series of metal electric potentials ϕ_M . The insets in (a) (b) and (d) present an enlarged view near the metal surface. With the potential of zero charge as the reference, the metal electric potential varies from -0.604 V ($U_M=1170$) to 0.939 V ($U_M=1230$) (every $10k_B T/e_0 = 0.257$ V).

3.2 Surface charging relation and double layer capacitance

The excess free charge density of the EDL is defined as,⁵⁰

$$\sigma_M = \int_{-\infty}^{\infty} (\bar{n}_{mc}(x) - \bar{n}_e(x))(a_0)^{-3} e_0 dx, \quad (36)$$

where $(a_0)^{-3}$ is the reference number density. As the whole EDL is electroneutral, σ_M is the negative of the net charge stored in the double layer,

$$\sigma_M = - \int_{-\infty}^{\infty} (z_c \bar{n}_c(x) + z_a \bar{n}_a(x))(a_0)^{-3} e_0 dx. \quad (37)$$

Figure 6 (a) shows σ_M as a function of ϕ_M for two electrolyte concentrations. σ_M increases monotonically from negative to positive values as ϕ_M increases. The electric potential at which $\sigma_M = 0$ is termed the potential of zero charge (pzc). Of note, the so-called pzc obtained from DFT-based first-principles models is actually calculated from the electronic work function of an uncharged metal-solution interface.^{31, 33-35} In contrast, the present model is able to determine the pzc directly from the σ_M vs. ϕ_M curve.

The differential double-layer capacitance is calculated using,

$$C_{dl} = \partial \sigma_M / \partial \phi_M \quad (38)$$

which is, as shown in Figure 6 (b), a two-humped camel-shaped function of ϕ_M . The valley is called Gouy-Chapman minimum, a classical concept in electrochemistry.¹

The two peaks in the C_{dl} vs. ϕ_M curve signify the crowding of counterions in the diffuse layer when ϕ_M deviates substantially from the pzc, namely, when the EDL is highly electrified. The locations of the two peaks depend on the ion size and the electrolyte concentration. The asymmetry in the height of two peaks reflects different sizes of counterions. The smaller the counterions, the higher the peak, due to the fact that counterions can be packed more densely and at a closer distance from the interface in the EDL. It is worth noting that the C_{dl} vs. ϕ_M curve is still asymmetrical for the equal-sized case, which is attributed to metal electrons entering into the solution

compartment – an asymmetric effect, as revealed previously.⁵⁰ Herein, the anions (PF_6^-) have a smaller size than the hydrated cations (K^+). Consequently, the anionic peak found at more positive ϕ_M has a slightly higher magnitude than the cationic peak found at more negative ϕ_M . The anionic peak is diminished to certain extent by the metal electronic effects.

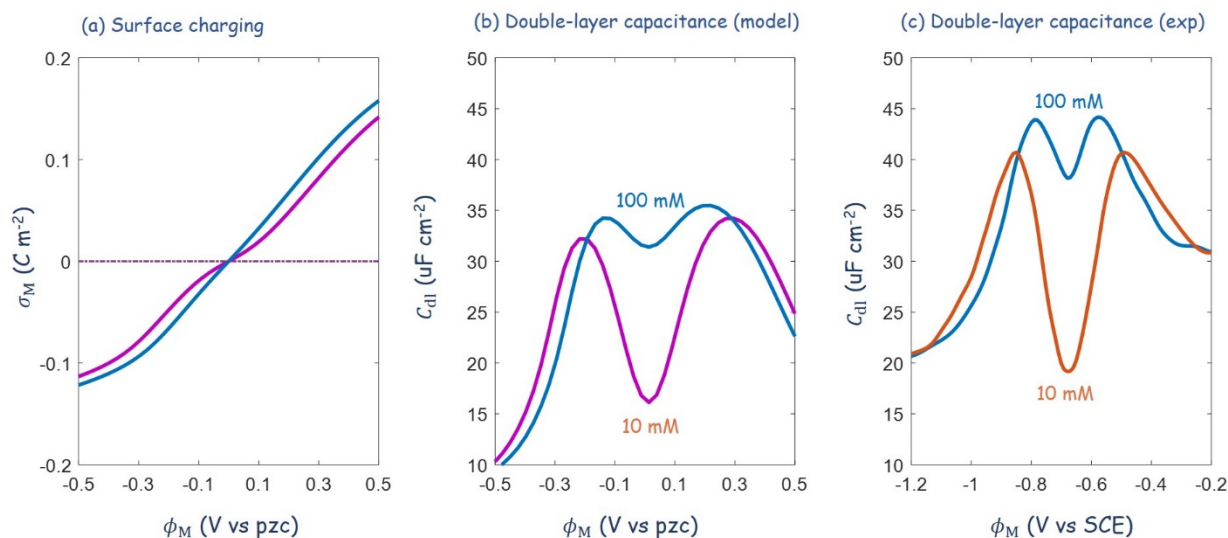


Figure 6. Model calculated (a) surface charging and (b) double layer capacitance of the EDL as a function of the metal electric potential for the Ag(111)- KPF_6 system. Two electrolyte concentrations (100 mM, 10 mM) are compared. The potential of zero charge is used as the potential reference. (c) Experimental capacitance curves measured by Valette on a Ag(111) electrode in 10 and 100 mM KPF_6 aqueous solution at room temperature. The electrode potential is referenced to the silver chloride electrode (SCE).⁷¹

Two electrolyte concentrations are compared in Figure 6 (b). It is found that the two peaks in the C_{dl} vs. ϕ_M curve are diminished and the distance between them decreases at higher concentration, which is a well-known feature of the Gouy-Chapman theory.^{7, 11} It is expected that the two peaks will eventually merge into a single peak as the

electrolyte concentration increases further. Under such circumstances, the two-humped camel-shaped curve transforms into a bell-shaped curve.¹¹ Experimental data measured by Valette for the Ag(111)-KPF₆ system at these two electrolyte concentrations are shown in Figure 6 (c). The experimental C_{dl} vs. ϕ_M curves were measured at a fixed frequency in the range between 20 and 320 Hz. The variation in the C_{dl} was found to be less than 5% in this frequency range, namely the frequency dispersion phenomenon is trivial. Valette demonstrated that the specific adsorption of PF₆⁻ is slight on Ag(111). Therefore, the contribution of the pseudo-capacitance of specific adsorption is small in the experiments. A reasonable agreement between the model and the experiment has been obtained, in terms of both the magnitude and the trend of the C_{dl} vs. ϕ_M curve, lending credence to the assumptions and parameters of the model.

3.3 Specific adsorption

Strong short-ranged electronic interactions may exist between metal surface and ions in solution, resulting in specific adsorption of ions (also termed chemisorption or electrosorption in the literature⁷²). As is known, electronic interactions broaden the electronic orbital of ions, causing partial electron transfer between the metal and ions and, consequently, resulting in partial charges on ions.⁷³⁻⁷⁴ In such circumstances, the charge numbers z_i in Eq.(6) are fractional and position- and potential dependent. The Schmickler-Kornyshev theory of electrosorption,⁷⁴⁻⁷⁵ which is based on the Anderson-Newns theory of chemisorption,^{57, 76} provides a formula for $z_i(r)$,

$$z_i = \pm \frac{1}{2} + \frac{1}{\pi} \arctan \left(\frac{\Delta H_i}{\Delta} \right), \quad (39)$$

where ΔH_i is the energy of the ion's highest occupied (for anions)/lowest unoccupied (for cations) molecular orbital relative to the Fermi level of the metal. Δ characterizes the strength of electronic interactions between metal surface and electrolyte ions. The

positive sign in front of 1/2 applies for cations and the negative sign for anions. A detailed derivation of Eq.(39) is provided in *Supporting Information*.

The strength of electronic interactions increases with decreasing distance of the ion to the metal surface. DFT calculations suggest an exponential relation,⁷⁷⁻⁷⁸

$$\Delta = \Delta_0 \exp(-\beta_1(x - l_M)h(x - l_M)) \quad (40)$$

where Δ_0 is the value at $x = l_M$, and β_1 an inverse length typically on the order of 1 \AA^{-1} ; $h(x)$ is the Heaviside function.

As the metal electric potential increases, the Fermi level decrease by $e_0\phi_M$, hence, ΔH_i increases by $e_0\phi_M$. Of note, ΔH_i also depends on the location of the ion. As a first approximation, we assume that near the metal surface ΔH_i varies linearly as a function of x , with a coefficient β_2 , thus giving

$$\Delta H_i = \Delta H_{i,\text{ref}} + e_0(\phi_M - \phi_{\text{ref}}) + \beta_2(x - l_M)h(x - l_M), \quad (41)$$

where $\Delta H_{i,\text{ref}}$ is the reference value at a given metal electric potential, ϕ_{ref} . In Eq.(41), ΔH_i will have very negative values when x keeps increasing, implying that z_a approaches -1 because Δ decreases exponentially.

Figure 7 shows results for the case of halogen ion electrosorption at Ag(111) with the following parameters: $\Delta H_{i,\text{ref}} = -10 k_B T$, $\phi_{\text{ref}} = 1200 k_B T/e_0$, $\Delta_0 = 20 k_B T$, $\beta_1 = 1 \text{ \AA}^{-1}$, $\beta_2 = -2 \text{ nm}^{-1}$. The anion loses its negative charge to a greater extent near the metal surface and with increasing ϕ_M , as described by Eq.(39) and shown in Figure 7 (a). The nonmonotonic spatial dependence of z_a results from the combination of an exponentially decaying Δ_0 and a linearly decreasing ΔH_i .

Partially charged anions are less effective in screening the positive free charge on the metal surface. Under such circumstance, solvent molecules will replace anions, resulting in an anomalous hump near the metal surface, as shown in Figure 7 (b). This phenomenon is termed surface depolarization of specifically adsorbing ions, which is expected to be general in the presence of ion specific adsorption.

The C_{dl} vs. ϕ_M curves of Ag(111) in 100 mM KCl (blue) and KI (red) are shown in Figure 7 (c). The potential of zero charge in the KCl solution, denoted pzc_{Cl} , is used as the potential reference. It is known that the specific adsorption of I^- is much stronger than that of Cl^- .⁷⁹ A stronger specific adsorption effectively brings the solution phase closer to the metal surface, as represented by smaller values of σ_t^1 and σ_t^2 in Eq.(8). Therefore, electronic interactions are intensified and Δ is larger, according to Eq.(40). In Figure 7 (c), we use $\sigma_t^1 = 2 \text{ \AA}$ for Cl^- and $\sigma_t^1 = 1 \text{ \AA}$ for I^- . The relation $\sigma_t^2 = \sigma_t^1/5$ is retained in both cases, so σ_t^2 is decreased proportionally.

The C_{dl} vs. ϕ_M curves change dramatically for the two halogen anions. Specifically, the C_{dl} vs. ϕ_M curve of I^- is shifted to the left and elevated significantly. Both features are observed in the experimental data measured by Valette, Hamelin and Parsons.⁷⁹ The pzc decreases by a magnitude of 0.4 V for I^- compared to Cl^- . This pzc shift reminds us that the pzc is co-determined by the electrode and the contacting electrolyte solution. Therefore, whenever discussing the pzc, one should specify the electrode and the contacting electrolyte solution on an equal footing. Both the pzc shift and the C_{dl} growth are ascribed to smaller values of σ_t^1 and σ_t^2 for the case with stronger ion specific adsorption. The Helmholtz capacitance is greater for a narrower metal-solution gap, resulting in the C_{dl} increase observed in Figure 7 (b). As a direct consequence of the larger C_{dl} , the pzc is obtained at a lower potential as ϕ_M increases from low to high values.

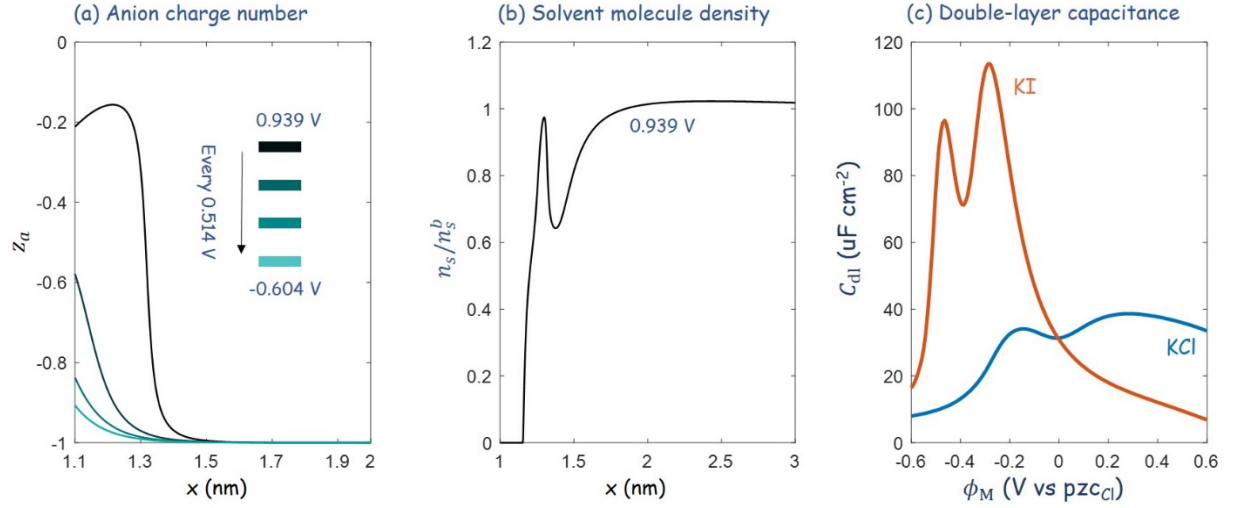


Figure 7. The EDL at Ag(111) in 100 mM KX (X=Cl and I) is calculated. The potential of zero charge in KCl, denoted pzc_{Cl} , is used as the potential reference. The partial charge transfer is modelled using $\Delta H_{i,\text{ref}} = -10 k_B T$, $\phi_{\text{ref}} = 1200 k_B T/e_0$, $\Delta_0 = 20 k_B T$, and $\beta_1 = 1 \text{ \AA}^{-1}$, $\beta_2 = -2 \text{ nm}^{-1}$. Other parameters for the case of Cl^- are listed in *Table 1*. The stronger specific adsorption of I^- leads to a narrow metal-solution gap, which is modelled using $\sigma_i^1 = 1 \text{ \AA}$ (c.f. $\sigma_i^1 = 2 \text{ \AA}$ for Cl^-). The relation $\sigma_i^2 = \sigma_i^1/5$ is retained in both cases. (a) Position-dependent charge number on Cl^- at a series of metal electric potentials. (b) Distribution of the solvent molecule density in the presence of Cl^- at 0.939 V. (c) Double-layer capacitance as a function of the metal electric potential for KCl (blue) and KI (red).

4 Concluding Remarks

We have formulated a hybrid density-potential functional to describe many-body interactions in the EDL in the grand-canonical ensemble. The model features: (1) the constant-potential description of the EDL, thus allowing the potential of zero charge to

be determined from the surface charging relation; (2) the consistent determination of the metal-solution gap which varies as a function of the electrode potential; (3) the treatment of ion specific adsorption and the accompanying partial charge transfer using the Anderson-Newns theory of chemisorption.

The model captures major electronic and electrostatic phenomena in the EDL, including oscillations of electron density and electric potential in the metal lattice, metal electron spillover, accumulation (depletion) of counterions (coions) in the diffuse layer, field-dependent orientation of solvent molecules, and partial charge transfer. For the case without electrosorption, it gives the typical two-humped camel-shaped curve of the differential double-layer capacitance (C_{dl}). A closer approach of the solution phase increases metal electron density in the solution compartment, which elevates the C_{dl} and decreases the pzc. In the case with consideration of electrosorption phenomena, partial charge transfer leads to the surface depolarization phenomenon.

From the perspective of accuracy and self-consistency, the presented fully analytical model has certain limitations. Firstly, the entire solution phase is treated classically at the mean-field level. Fluctuation effects and correlations are not considered.⁸⁰⁻⁸¹ Secondly, it uses empirical force relations describing the short-range interactions between the metal and solution particles, though the parameters in the empirical relations could be determined from DFT calculations. Thirdly, it employs the simple TFDW theory to describe metal electrons, which can be replaced with more advanced functionals (e.g. ref.⁸²). These will be important frontiers to expand upon in future work in theory and computation.

Acknowledgement

J.H. acknowledges the financial support from the Alexander von Humboldt Foundation and National Natural Science Foundation of China under the grant number of 21802170. ME acknowledges the financial support from Forschungszentrum Jülich GmbH.

Supporting Information

Comparison between the TFDW theory and modern DFT calculation for the Ag(111)-vacuum system; Electrostatic energy of solvent molecules; Solving the problem using Matlab; Schmickler-Kornyshev theory of electrosorption; Matlab code.

Notes

The authors declare no competing financial interest.

Reference

1. Bard, A. J.; Inzelt, G.; Scholz, F., *Electrochemical Dictionary*; Springer-Verlag: Berlin Heidelberg, 2008.
2. Helmholtz, H. V., Studien Über Electriche Grenzschichten. *Ann. Phys.* **1879**, 243, 337-382.
3. Gouy, G., Sur La Constitution De La Charge Electrique a La Surface D'un Electrolyte. *J. Phys. Theor. Appl.* **1910**, 9, 457–468.
4. Chapman, D. L., Li. A Contribution to the Theory of Electrocapillarity. *Phil. Mag.* **1913**, 25, 475-481.
5. Stern, O., Zur Theorie Der Elektrolytischen Doppelschicht. *Ber. Bunsenges. Phys. Chem.* **1924**, 30, 508-516.
6. Bikerman, J. J., Xxxix. Structure and Capacity of Electrical Double Layer. *Lond. Edinb. Dubl. Phil. Mag.* **1942**, 33, 384-397.
7. Grahame, D. C., The Electrical Double Layer and the Theory of Electrocapillarity. *Chem. Rev.* **1947**, 41, 441-501.

8. Bockris, J. O. M.; Devanathan, M. A. V.; Müller, K., On the Structure of Charged Interfaces. *Proc. Roy. Soc. A* **1963**, 274, 55-79.
9. Parsons, R., The Electrical Double Layer: Recent Experimental and Theoretical Developments. *Chem. Rev.* **1990**, 90, 813-826.
10. Borukhov, I.; Andelman, D.; Orland, H., Steric Effects in Electrolytes: A Modified Poisson-Boltzmann Equation. *Phys. Rev. Lett.* **1997**, 79, 435-438.
11. Kornyshev, A. A., Double-Layer in Ionic Liquids: Paradigm Change? *J. Phys. Chem. B* **2007**, 111, 5545-5557.
12. Bazant, M.; D Storey, B.; Kornyshev, A., Double Layer in Ionic Liquids: Overscreening Versus Crowding. *Phys. Rev. Lett.* **2011**, 106, 046102.
13. Damaskin, B. B.; Petrii, O. A., Historical Development of Theories of the Electrochemical Double Layer. *J. Solid State Electrochem.* **2011**, 15, 1317-1334.
14. Huang, J.; Malek, A.; Zhang, J.; Eikerling, M. H., Non-Monotonic Surface Charging Behavior of Platinum: A Paradigm Change. *J. Phys. Chem. C* **2016**, 120, 13587-13595.
15. Huang, J.; Zhou, T.; Zhang, J.; Eikerling, M., Double Layer of Platinum Electrodes: Non-Monotonic Surface Charging Phenomena and Negative Double Layer Capacitance. *J. Chem. Phys.* **2018**, 148, 044704.
16. Badiali, J. P.; Rosinberg, M. L.; Goodisman, J., Contribution of the Metal to the Differential Capacity of an Ideally Polarisable Electrode. *J. Electroanal. Chem.* **1983**, 143, 73-88.
17. Badiali, J. P.; Rosinberg, M. L.; Vericat, F.; Blum, L., A Microscopic Model for the Liquid Metal-Ionic Solution Interface. *J. Electroanal. Chem.* **1983**, 158, 253-267.
18. Schmickler, W., A Jellium-Dipole Model for the Double Layer. *J. Electroanal. Chem.* **1983**, 150, 19-24.
19. Schmickler, W.; Henderson, D., The Interphase between Jellium and a Hard Sphere Electrolyte. A Model for the Electric Double Layer. *J. Chem. Phys.* **1984**, 80, 3381-3386.
20. Feldman, V. I.; Kornyshev, A. A.; Partenskiĭ, M. B., Density Functional Simulation of Interfacial Relaxation and Capacity of a Model Metal/Electrolyte Interface. *Solid State Commun.* **1985**, 53, 157-164.

21. Feldman, V. J.; Partenskii, M. B.; Vorob'ev, M. M., Surface Electron Screening Theory and Its Applications to Metal-Electrolyte Interfaces. *Prog. Surf. Sci.* **1986**, 23, 3-154.
22. Schmickler, W.; Henderson, D., The Interphase between Jellium and a Hard Sphere Electrolyte: Capacity–Charge Characteristics and Dipole Potentials. *J. Chem. Phys.* **1986**, 85, 1650-1657.
23. Badiali, J. P., The Jellium Model in Electrochemistry. *Ber. Bunsenges. Phys. Chem.* **1987**, 91, 270-276.
24. Amokrane, S.; Russier, V.; Badiali, J. P., A Model for the Metal-Solvent Coupling at a Charged Interface: Effect on the Differential Capacitance. *Surf. Sci.* **1989**, 210, 251-270.
25. Kim, Z. B.; Kornyshev, A. A.; Partenskii, M. B., On the Anomalously High and Negative Values of the Compact Layer Capacity in Some New Models of the Metal/Electrolyte Interface. *J. Electroanal. Chem.* **1989**, 265, 1-9.
26. Kornyshev, A. A., Metal Electrons in the Double Layer Theory. *Electrochim. Acta* **1989**, 34, 1829-1847.
27. Kornyshev, A. A.; Kuznetsov, A. M.; Makov, G.; Vigdorovitch, M. V., Polaron Effects on Electronic Properties of Metal/Medium Interfaces. Part 1.—Uncharged Metal/Dielectric and Metal/Electrolyte Interfaces. *J. Chem. Soc. Faraday Trans.* **1996**, 92, 3997-4004.
28. Kornyshev, A. A.; Kuznetsov, A. M.; Makov, G.; Vigdorovitch, M. V., Polaron Effects on Electronic Properties of Metal/Medium Interfaces. Part 2.—Electrified Interfaces: In Situ Second Harmonic Generation. *J. Chem. Soc. Faraday Trans.* **1996**, 92, 4005-4014.
29. Schmickler, W., Electronic Effects in the Electric Double Layer. *Chem. Rev.* **1996**, 96, 3177-3200.
30. Jinnouchi, R.; Anderson, A. B., Electronic Structure Calculations of Liquid-Solid Interfaces: Combination of Density Functional Theory and Modified Poisson-Boltzmann Theory. *Phys. Rev. B* **2008**, 77, 245417.
31. Tripkovic, V.; Björketun, M. E.; Skúlason, E.; Rossmeisl, J., Standard Hydrogen Electrode and Potential of Zero Charge in Density Functional Calculations. *Phys. Rev. B* **2011**, 84, 115452.

32. Letchworth-Weaver, K.; Arias, T. A., Joint Density Functional Theory of the Electrode-Electrolyte Interface: Application to Fixed Electrode Potentials, Interfacial Capacitances, and Potentials of Zero Charge. *Phys. Rev. B* **2012**, *86*, 075140.
33. Sakong, S.; Forster-Tonigold, K.; Groß, A., The Structure of Water at a Pt(111) Electrode and the Potential of Zero Charge Studied from First Principles. *J. Chem. Phys.* **2016**, *144*, 194701.
34. Le, J.; Iannuzzi, M.; Cuesta, A.; Cheng, J., Determining Potentials of Zero Charge of Metal Electrodes Versus the Standard Hydrogen Electrode from Density-Functional-Theory-Based Molecular Dynamics. *Phys. Rev. Lett.* **2017**, *119*, 016801.
35. Sakong, S.; Groß, A., The Electric Double Layer at Metal-Water Interfaces Revisited Based on a Charge Polarization Scheme. *J. Chem. Phys.* **2018**, *149*, 084705.
36. Magnussen, O. M.; Groß, A., Toward an Atomic-Scale Understanding of Electrochemical Interface Structure and Dynamics. *J. Am. Chem. Soc.* **2019**, *141*, 4777-4790.
37. Sakong, S.; Groß, A., Water Structures on a Pt(111) Electrode from Ab Initio Molecular Dynamic Simulations for a Variety of Electrochemical Conditions. *Phys. Chem. Chem. Phys.* **2020**, *22*, 10431-10437.
38. Nishihara, S.; Otani, M., Hybrid Solvation Models for Bulk, Interface, and Membrane: Reference Interaction Site Methods Coupled with Density Functional Theory. *Phys. Rev. B* **2017**, *96*, 115429.
39. Liu, J.; Huang, J., A Mean-Field Model for the Double Layer of Stepped Platinum Single-Crystal Electrodes. *J. Electroanal. Chem.* **2019**, *846*, 113136.
40. Booth, F., The Dielectric Constant of Water and the Saturation Effect. *J. Chem. Phys.* **1951**, *19*, 391-394.
41. Gongadze, E.; Iglič, A., Decrease of Permittivity of an Electrolyte Solution near a Charged Surface Due to Saturation and Excluded Volume Effects. *Bioelectrochemistry* **2012**, *87*, 199-203.
42. Goodwin, Z. A. H.; Feng, G.; Kornyshev, A. A., Mean-Field Theory of Electrical Double Layer in Ionic Liquids with Account of Short-Range Correlations. *Electrochim. Acta* **2017**, *225*, 190-197.
43. Downing, R.; Bossa, G. V.; May, S., The Role of Ion-Ion Correlations for the Differential Capacitance of Ionic Liquids. *J. Phys. Chem. C* **2018**, *122*, 28537-28544.

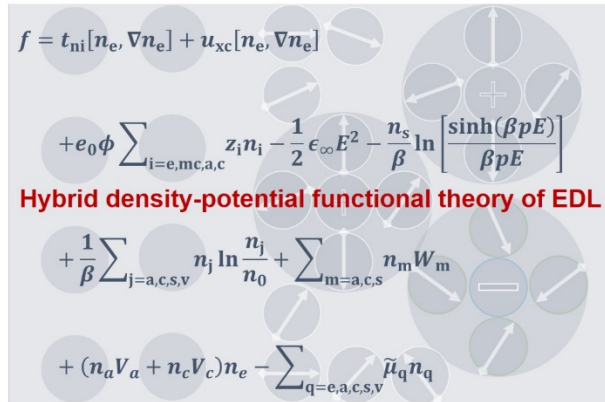
44. Lang, N. D.; Kohn, W., Theory of Metal Surfaces: Charge Density and Surface Energy. *Phys. Rev. B* **1970**, *1*, 4555-4568.
45. Lang, N. D., The Density-Functional Formalism and the Electronic Structure of Metal Surfaces. In *Solid State Phys.*, Ehrenreich, H.; Seitz, F.; Turnbull, D., Eds. Academic Press: 1974; Vol. 28, pp 225-300.
46. Perdew, J. P.; Kurth, S., Density Functionals for Non-Relativistic Coulomb Systems in the New Century. In *A Primer in Density Functional Theory*, Fiolhais, C.; Nogueira, F.; Marques, M. A. L., Eds. Springer Berlin Heidelberg: Berlin, Heidelberg, 2003; pp 1-55.
47. Melander, M. M.; Kuisma, M. J.; Christensen, T. E. K.; Honkala, K., Grand-Canonical Approach to Density Functional Theory of Electrocatalytic Systems: Thermodynamics of Solid-Liquid Interfaces at Constant Ion and Electrode Potentials. *J. Chem. Phys.* **2018**, *150*, 041706.
48. Melander, M. M., Grand Canonical Rate Theory for Electrochemical and Electrocatalytic Systems I: General Formulation and Proton-Coupled Electron Transfer Reactions. *J. Electrochem. Soc.* **2020**, *167*, 116518.
49. Eslamibidgoli, M. J.; Eikerling, M. H., Approaching the Self-Consistency Challenge of Electrocatalysis with Theory and Computation. *Curr. Opin. Electrochem.* **2018**, *9*, 189-197.
50. Huang, J.; Li, P.; Chen, S., Potential of Zero Charge and Surface Charging Relation of Metal-Solution Interphases from a Constant-Potential Jellium-Poisson-Boltzmann Model. *Phys. Rev. B* **2020**, *101*, 125422.
51. Huang, K., *Statistical Mechanics*, Second edition ed.; John Wiley & Sons: New York, 1987.
52. Lundqvist, S.; March, N. H., *Theory of the Inhomogeneous Electron Gas*; Springer Science & Business Media, 2013.
53. Thomas, L. H., The Calculation of Atomic Fields. *Math. Proc. Camb. Phil. Soc.* **1927**, *23*, 542-548.
54. Fermi, E., Eine Statistische Methode Zur Bestimmung Einer Eigenschaft Des Atoms Und Ihre Anwendung Auf Die Theorie Des Periodischen Systems Der Elemente. *Z. Phys.* **1928**, *48*, 73-79.
55. Wigner, E., On the Interaction of Electrons in Metals. *Phys. Rev.* **1934**, *46*, 1002-1011.

56. Smith, J. R., Self-Consistent Many-Electron Theory of Electron Work Functions and Surface Potential Characteristics for Selected Metals. *Phys. Rev.* **1969**, *181*, 522-529.
57. Anderson, P. W., Localized Magnetic States in Metals. *Phys. Rev.* **1961**, *124*, 41-53.
58. Muscat, J. P.; Newns, D. M., Chemisorption on Metals. *Prog. Surf. Sci.* **1978**, *9*, 1-43.
59. Budkov, Y. A., Nonlocal Statistical Field Theory of Dipolar Particles in Electrolyte Solutions. *J. Phys. Condens. Matt.* **2018**, *30*, 344001.
60. Budkov, Y. A., Statistical Field Theory of Ion–Molecular Solutions. *Phys. Chem. Chem. Phys.* **2020**, *22*, 14756-14772.
61. Wick, C. D.; Xantheas, S. S., Computational Investigation of the First Solvation Shell Structure of Interfacial and Bulk Aqueous Chloride and Iodide Ions. *J. Phys. Chem. B* **2009**, *113*, 4141-4146.
62. Mähler, J.; Persson, I., A Study of the Hydration of the Alkali Metal Ions in Aqueous Solution. *Inorg. Chem.* **2012**, *51*, 425-438.
63. Takeuchi, M.; Matubayasi, N.; Kameda, Y.; Minofar, B.; Ishiguro, S.-i.; Umebayashi, Y., Free-Energy and Structural Analysis of Ion Solvation and Contact Ion-Pair Formation of Li⁺ with Bf₄[−] and Pf₆[−] in Water and Carbonate Solvents. *J. Phys. Chem. B* **2012**, *116*, 6476-6487.
64. Zhang, Y.; Huang, J., Treatment of Ion-Size Asymmetry in Lattice-Gas Models for Electrical Double Layer. *J. Phys. Chem. C* **2018**, *122*, 28652-28664.
65. Kierzenka, J.; Shampine, L. F., A Bvp Solver Based on Residual Control and the Matlab Pse. *ACM Trans. Math. Software* **2001**, *27*, 299–316.
66. Fattebert, J.-L.; Gygi, F., Density Functional Theory for Efficient Ab Initio Molecular Dynamics Simulations in Solution. *J. Comput. Chem.* **2002**, *23*, 662-666.
67. Otani, M.; Sugino, O., First-Principles Calculations of Charged Surfaces and Interfaces: A Plane-Wave Nonrepeated Slab Approach. *Phys. Rev. B* **2006**, *73*, 115407.
68. Bramley, G.; Nguyen, M.-T.; Glezakou, V.-A.; Rousseau, R.; Skylaris, C.-K., Reconciling Work Functions and Adsorption Enthalpies for Implicit Solvent Models: A Pt (111)/Water Interface Case Study. *J. Chem. Theory Comput.* **2020**, *16*, 2703-2715.

69. Heenen, H. H.; Gauthier, J. A.; Kristoffersen, H. H.; Ludwig, T.; Chan, K., Solvation at Metal/Water Interfaces: An Ab Initio Molecular Dynamics Benchmark of Common Computational Approaches. *J. Chem. Phys.* **2020**, *152*, 144703.
70. Fernandez-Alvarez, V. M.; Eikerling, M. H., Interface Properties of the Partially Oxidized Pt(111) Surface Using Hybrid Dft–Solvation Models. *ACS Appl. Mater. Interfaces* **2019**, *11*, 43774-43780.
71. Valette, G., Double Layer on Silver Single Crystal Electrodes in Contact with Electrolytes Having Anions Which Are Slightly Specifically Adsorbed: Part Iii. The (111) Face. *J. Electroanal. Chem.* **1989**, *269*, 191-203.
72. Schmickler, W.; Guidelli, R., The Partial Charge Transfer. *Electrochim. Acta* **2014**, *127*, 489-505.
73. Huang, J., Mixed Quantum-Classical Treatment of Electron Transfer at Electrocatalytic Interfaces: Theoretical Framework and Conceptual Analysis. *J. Chem. Phys.* **2020**, *153*, 164707.
74. Kornyshev, A. A.; Schmickler, W., On the Coverage Dependence of the Partial Charge Transfer Coefficient. *J. Electroanal. Chem.* **1986**, *202*, 1-21.
75. Schmickler, W., A Model for the Charge Transfer to Alkali Adsorbates. *J. Electroanal. Chem.* **1979**, *100*, 533-546.
76. Newns, D. M., Self-Consistent Model of Hydrogen Chemisorption. *Phys. Rev.* **1969**, *178*, 1123-1135.
77. Santos, E.; Lundin, A.; Pötting, K.; Quaino, P.; Schmickler, W., Model for the Electrocatalysis of Hydrogen Evolution. *Phys. Rev. B* **2009**, *79*, 235436.
78. Huang, J.; Li, P.; Chen, S., Quantitative Understanding of the Sluggish Kinetics of Hydrogen Reactions in Alkaline Media Based on a Microscopic Hamiltonian Model for the Volmer Step. *J. Phys. Chem. C* **2019**, *123*, 17325-17334.
79. Valette, G.; Hamelin, A.; Parsons, R., Specific Adsorption on Silver Single Crystals in Aqueous Solutions. *Z. Phys. Chem.* **1978**, *113*, 71-89.
80. Podgornik, R., Electrostatic Correlation Forces between Surfaces with Surface Specific Ionic Interactions. *J. Chem. Phys.* **1989**, *91*, 5840-5849.
81. Netz, R. R.; Orland, H., Beyond Poisson-Boltzmann: Fluctuation Effects and Correlation Functions. *Eur. Phys. J. E* **2000**, *1*, 203-214.

82. Perdew, J. P.; Burke, K.; Ernzerhof, M., Generalized Gradient Approximation Made Simple. *Phys. Rev. Lett.* **1996**, 77, 3865-3868.

TOC Graphic



The TOC graphic features a light gray background with a pattern of overlapping circles. Some circles contain mathematical symbols: a plus sign (+), a minus sign (-), and a multiplication sign (×). Arrows of varying lengths and directions are scattered throughout the graphic, pointing towards the central text and equations.

$$f = t_{\text{ni}}[n_e, \nabla n_e] + u_{\text{xc}}[n_e, \nabla n_e]$$

$$+ e_0 \phi \sum_{i=e,mc,a,c} z_i n_i - \frac{1}{2} \epsilon_{\infty} E^2 - \frac{n_s}{\beta} \ln \left[\frac{\sinh(\beta p E)}{\beta p E} \right]$$

Hybrid density-potential functional theory of EDL

$$+ \frac{1}{\beta} \sum_{j=a,c,s,v} n_j \ln \frac{n_j}{n_0} + \sum_{m=a,c,s} n_m W_m$$

$$+ (n_a V_a + n_c V_c) n_e - \sum_{q=e,a,c,s,v} \tilde{\mu}_q n_q$$